Contents lists available at ScienceDirect

Journal of Colloid and Interface Science

journal homepage: www.elsevier.com/locate/jcis

Poly (diglycerol adipate) variants as enhanced nanocarrier replacements in drug delivery applications

Philippa L. Jacob [a], Benedetta Brugnoli [b], Alessandra Del Giudice [b], Hien Phan [c], Veeren M. Chauhan [d],
Laura Beckett [d], Richard B. Gillis [e,f,g], Cara Moloney [h], Robert J. Cavanagh [h], Eduards Krumins [a],
Morgan Reynolds-Green [a], Joachim C. Lentz [a], Claudia Conte [i], Valentina Cuzzucoli Crucitti [j],
Benoit Couturaud [c], Luciano Galantini [b], Iolanda Francolini [b], Steven M. Howdle [a], Vincenzo Taresco [a,*]

[a] School of Chemistry, University Park, Nottingham NG7 2RD, United Kingdom
[b] Dept. of Chemistry, Sapienza University of Rome, Piazzale A. Moro 5, 00185 Rome, Italy
[c] Institut de Chimie et des Matériaux Paris-Est, Université de Paris-Est Créteil, CNRS UMR 7182, 2 rue Henri Dunant, 94320 Thiais, France
[d] Laboratory of Biophysics and Surface Analysis, School of Pharmacy, University of Nottingham, Boots Sciences Building, University Park, Nottingham NG7 2RD, United Kingdom
[e] National Centre for Macromolecular Hydrodynamics, University of Nottingham, Sutton Bonington LE12 5RD, United Kingdom
[f] Biomaterials Group, School of Biosciences, University of Nottingham, Sutton Bonington LE12 5RD, United Kingdom
[g] College of Business, Technology and Engineering, Sheffield Hallam University, Food and Nutrition Group, Sheffield S1 1WB, United Kingdom
[h] School of Medicine, BioDiscovery Institute-3, University Park, Nottingham NG7 2RD, United Kingdom
[i] Department of Pharmacy, University of Napoli Federico II, Napoli, Italy
[j] Centre for Additive Manufacturing and Department of Chemical and Environmental Engineering, Faculty of Engineering, University of Nottingham, Nottingham NG7 2RD, United Kingdom

GRAPHICAL ABSTRACT
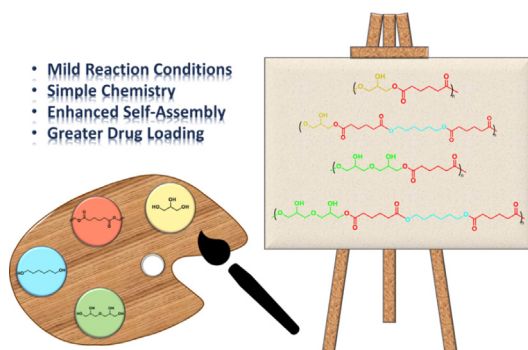
- Mild Reaction Conditions
- Simple Chemistry
- Enhanced Self-Assembly
- Greater Drug Loading

ARTICLE INFO

ABSTRACT

Sustainably derived poly(glycerol adipate) (PGA) has been deemed to deliver all the desirable features expected in a polymeric scaffold for drug-delivery, including biodegradability, biocompatibility, self-assembly into nanoparticles (NPs) and a functionalisable pendant group. Despite showing these advantages over commercial alkyl polyesters, PGA suffers from a series of key drawbacks caused by poor amphiphilic balance. This leads to weak drug-polymer interactions and subsequent low drug-loading in NPs, as well as low NPs stability. To overcome this, in the present work, we applied a more significant variation of the polyester backbone while maintaining mild and sustainable polymerisation conditions. We have investigated the effect of the variation of both hydrophilic and hydrophobic segments upon physical properties and drug interactions as well as self-assembly and NPs stability. For the first time

* Corresponding author.
  E-mail address: vincenzo.taresco@nottingham.ac.uk (V. Taresco).

we have replaced glycerol with the more hydrophilic diglycerol, as well as adjusting the final amphiphilic balance of the polyester repetitive units by incorporating the more hydrophobic 1,6-*n*-hexanediol (Hex). The properties of the novel poly(diglycerol adipate) (PDGA) variants have been compared against known polyglycerol-based polyesters. Interestingly, while the bare PDGA showed improved water solubility and diminished self-assembling ability, the Hex variation demonstrated enhanced features as a nanocarrier. In this regard, PDGAHex NPs were tested for their stability in different environments and for their ability to encode enhanced drug loading. Moreover, the novel materials have shown good biocompatibility in both *in vitro* and *in vivo* (whole organism) experiments.

1. Introduction

The application of polymeric nanomaterials as vehicles for drug delivery is a rapidly expanding area of research, with over 1600 articles published on this topic in 2021 (source Web of Science).[1] Polymers used in these applications should preferably be biodegradable but most importantly biocompatible.[2] They should ideally be multifunctional or be able to allow the introduction of novel functionalities, along their backbones or side chains. They should self-assemble in aqueous environments and, at the same time they should encode for the highest drug loading through encapsulation.[3-5] Whilst polyethylene glycol (PEG) based polymers are widely used in many drug formulations, they are not readily biodegraded in the body and their overuse has been shown to cause bioaccumulation as well as PEG antibody formation within the population[6,7]. The consequences of this include hypersensitivity, faster drug clearance and occasionally life-threatening side effects.[6,7] In addition to this, the synthesis of PEG includes the use and production of hazardous chemicals. For example, the anionic polymerisation of ethylene oxide, a known carcinogen, produces 1,4-dioxane as a by-product, which is a suspected carcinogenic compound.[7,8].

Polyesters present an alternative, biodegradable solution to this challenge.[3] Many polyesters can be readily hydrolysed in physiological conditions and have been shown to be useful in drug delivery applications including polyglycolic acid and polycaprolactone.[9] Polyglycolic acid has been shown to have the key properties required to make a suitable material for nanoparticle (NPs) formulation and drug encapsulation.[10] Its monomeric precursor, glycolic acid is typically synthesised via the hydrolysis of chloroacetic acid (highly toxic and corrosive) and on an industrial scale is typically petrochemical derived.[11,12] Recent developments by Pujing Chemical Industry Limited Co. have demonstrated that the production of polyglycolic acid can be made more environmentally friendly on an industrial scale by avoiding the use of toxic chemicals and utilising industrial by-products in the synthesis.[11,12].

Polylactic acid (PLA) is an example of a sustainably derived, biodegradable polyester.[13] Different PLA-containing products are FDA approved and have been extensively shown to facilitate the targeted delivery of hydrophobic drugs.[14] However, there are several limitations associated with the use of PLA in drug delivery applications including a lack of backbone functionality to facilitate cell specific interactions, as well as low loading efficiencies with hydrophilic compounds (e.g. proteins) due to the hydrophobic nature of the polymer.[15] PLA is commonly used in block copolymers to overcome these limitations, often in combination with PEG.[3].

Poly(lactic-*co*-glycolic acid) (PLGA) is composed of both lactic and glycolic acid monomers and has a degradation profile that can be finely tuned according to its intended application.[14] PLGA NPs have been widely shown to be proficient in the encapsulation and targeted delivery of both hydrophobic and hydrophilic molecules.[16] Whilst this polymer has been shown to be very effective for targeted drug delivery, surfactants and stabilisers are often required in the formulations, some of which have reported side effects including toxicity.[16].

Other literature examples of bioderived and biodegradable polyesters used in drug delivery include jasmine lactone derived polymers[17] and polyhydroxyalkanoates[3]. However, many of these polymers require multiple step synthesis and have not yet been shown to be scalable. Therefore, there is an academic and industrial driving force to expand the library of biocompatible and bioderived polymers.[18,19].

Poly(glycerol adipate) (PGA) is a glycerol derived biodegradable and biocompatible polyester that has been shown to be a polymer highly suited to drug delivery applications.[20-22] Glycerol, a by-product of biodiesel production, is produced on an enormous scale, predicted to exceed 4000 million litres per year by 2026.[23] With limited large-scale industrial applications of this polyol, there is a broad interest in developing applications. PGA can be enzymatically synthesised in a one-pot reaction using a lipase enzyme (Novozym 435), known to be selective to primary alcohols. This enables the synthesis of linear polyesters with minimal branching of the tertiary glycerol hydroxyl group, leaving the pendant hydroxyl groups largely unreacted.[21,24] In addition to being a sustainably derived polyester, PGA is capable of self-assembling due to its well-balanced amphiphilicity, aided by the pendant hydroxyl groups.[25-27] Literature examples have shown that PGA can self-assemble into non-toxic NPs of around 100 nm in size, without the requirement of additional (often PEG-based) surfactants or additives to stabilise the NPs.[27-29].

Whilst PGA can self-assemble into NPs without the use of surfactants, previous work by multiple researchers shows that PGA NPs can be stabilised by the addition of fatty acids onto the polymer backbone through an esterification of the pendant hydroxyl group.[27,30,31] Furthermore, the addition of other drug like molecules onto the polymer backbone via esterification has been utilised to synthesise polymeric pro-drugs that are capable of self-assembly into stable NPs, with good efficacy.[26,32] Steglich esterifications have been frequently used in literature as an efficient route to polymeric pro-drugs and modified polymer backbones. However, there are several disadvantages associated with the Steglich esterification modification route including long reaction times, multiple purification steps and the use of toxic reagents.

Recently, Jacob et al. introduced a novel approach to PGA modifications by introducing a second diol into the polymer backbone in a one-pot enzymatic reaction.[28] This alternative method of introducing an extra functionality avoids the use of toxic coupling reagents and requires minimal purification steps. At the same time, pendant hydroxyl groups on the polymer backbone which are vital for self-assembly are maintained.[33].

To further investigate the effect of amphiphilic balance on the self-assembly and stability of NPs, the physical properties and drug interactions, variation of both hydrophilic and hydrophobic

segments of PGA was carried out. In the present work, for the first time, we have replaced glycerol with a glycerol derivative – diglycerol and adjusted the final amphiphilic balance of the polyester repetitive units by incorporating the more hydrophobic 1,6-*n*-hexanediol (Hex). Although very similar to glycerol, it is synthesised industrially using epichlorohydrin via the Epicerol process developed by Solvay, producing 100% biobased epichlorohydrin. [23] The greener synthesis of this starting material highlights diglycerol as a monomer capable of introducing additional hydrophilicity into polymer backbones in a facile manner.

Herein, we report the synthesis of a novel class of polyesters – poly(diglycerol adipate) (PDGA) and its modification with 1,6-*n*-hexanediol (PDGAHex). The properties of the novel poly(diglycerol adipate) variants have been compared against known polyglycerol-based polyesters. PDGAHex, in particular, has shown superior physical properties as well as enhanced properties essential for application in drug delivery compared with previously studied PGA derived polymers.

2. Experimental section

2.1. Materials and methods

Novozym 435 lipase, derived from *Candida antarctica* immobilised on an acrylic macroporous resin, glycerol, diglycerol and 1,6-*n*-hexanediol were purchased from Sigma-Aldrich, UK. Divinyl adipate was purchased from Tokyo Chemical Industries, UK. All Chemicals were used as received without further purification. Solvents were purchased from Fisher Scientific UK and were used without further purification.

2.2. Characterisation

2.2.1. Nuclear magnetic resonance spectroscopy (NMR)

Successful polymer synthesis and repeat unit structure were confirmed using ^{1}H NMR spectroscopy. NMR spectra were recorded using a Bruker DPX 400 MHz spectrometer using acetone d_6 solvent. Chemical shifts are given in ppm.

2.2.2. Gel permeation chromatography (GPC)

Polymer molecular weight and polydispersity were determined using GPC in THF (HPLC grade) eluent at 40 °C. Chromatographs were recorded using two Agilent PL-gel mixed D columns in series with a flow rate of 1 mL min^{-1} and an injection loop of 50 μL. Samples were detected using a differential refractometer (DRI). Samples were prepared by dissolving sample (6 mg) in THF (2 mL) and filtering through 0.22 μM Teflon filter. Poly(methyl methacrylate) samples were used for the system calibration with average molecular weights ranging from 540 to 1.02×10^6 g mol^{-1} and dispersity (Đ) of approximately 1.

2.2.3. Differential scanning calorimetry (DSC)

Thermal properties of the polymers were measured using DSC. Analysis was performed on a TA-Q2000 (TA instruments), calibrated with sapphire and indium standards under N$_2$ flow at 50 mL min^{-1}. Polymer (~5 mg) was weighted into a *T*-zero aluminium pan (TA instruments) with a reference pan (*T*-zero aluminium) remaining empty. Pan lids were pin-holed, and samples were heated at a rate of 20 °C min^{-1} from −90 to 200 °C. Two heating cycles were recorded in order to remove any thermal history of the polymers. The second heating cycle was used to determine the glass transition temperature (T_g) and melting temperature (T_m) of polymers.

2.2.4. Dynamic light scattering (DLS) and zeta potential measurements

Dynamic light scattering was used to determine NPs size using a Zetasizer Nano spectrometer (Malvern Instruments Ltd.) equipped with a 633 nm laser at a fixed angle of 173°. Samples were equilibrated for 30 s at 25 °C prior to measurement. Zetasizer Nano spectrometer was also used to measure zeta-potential of the NPs. All samples were measured in triplicate. NPs were prepared at a concentration of 2.5 mg/mL and filtered through 0.22 μM filter.

2.2.5. Water contact angle measurement (θ_w)

Water contact angle samples were prepared by solvent casting of polymer in a solution of acetone onto microscopic glass slides. Samples were prepared at a concentration of 3 mg/mL. Water contact angles were measured using a KSV Cam 200 (KSV Instruments Ltd, Helsinki, Finland) equipped with CAM200 software. Samples were measured at a constant temperature (25 °C) with four replicates of each measurement recorded.

2.2.6. CAC measurements

Critical Aggregation Concentration (CAC) was evaluated using a Zetasizer Nano ZS as previously reported.[34] A constant attenuator was chosen from the highest solution concentration (1000 μg/mL). The count rate (kcps) intensity decreases from the highest to the lowest dilution (1000–1.00 μg/mL) until reaching a plateau. CAC was then calculated by plotting intensity (kcps) against concentration (μg/mL) and intersecting the two lines.[35].

2.2.7. Transmission electron microscopy (TEM) measurements

NP dispersions (13 μL, 2 mg/mL) were added to a copper grid (Carbon film 200 mesh copper (Agar Scientific)) and left for 2 min after which time the excess sample was removed. The TEM grids were left to dry for 3 h before measuring. Analysis was performed using a FEI Biotwin-12 TEM fitted with a digital camera.

2.2.8. Rheological measurements

Rheological measurements were performed on an Anton Paar MCR102X Rheometer equipped with a 25 mm parallel plate geometry. Measurements were carried out at a gap of 1 mm and 25 °C.

2.2.9. Analytical ultracentrifugation

Analytical ultracentrifugation (AUC) was carried out using a Beckman XL-I (Indiana, USA). Samples were dissolved at 10% concentration in PBS 0.1 M at pH 7 and loaded into the chamber of cells constructed from Al-epon centrepieces, sapphire windows and aluminium housing. The solvent channel was filled with PBS. Samples were centrifuged at 50 k rpm and scanned with interference optics until no further movement was observed.

Sedimentation equilibrium data (AUC-SE) were analysed using SEDFIT-MSTAR,[36] using a partial specific volume of 0.82 mL/g, [37] and the built in c(M) algorithm to fit baseline.

2.2.10. Small angle X-ray scattering

The X-ray scattering measurements were performed at SAXSLab Sapienza with a Xeuss 2.0 Q Xoom system (Xenocs SAS, Grenoble, France) equipped with a micro-focus Genix 3D X-ray Cu source (λ = 0.1542 nm) and a two-dimensional Pilatus3 R 300 K detector placed at a variable distance from the sample (Dectris Ltd., Baden, Switzerland). The beam size was defined through the two-pinhole collimation system equipped with "scatterless" slits to be 0.5 mm × 0.5 mm. Calibration of the scattering vector modulus q range, where q=($4\pi \sin\theta)/\lambda$, 2θ being the scattering angle, was performed using silver behenate. The solutions of the polymers dissolved in acetone (10 mg/ml) and the polymer NPs obtained by nanoprecipitation in water (2.5 mg/ml, and then filtered through 0.22 μM filter) were loaded into disposable borosilicate glass capillaries and

sealed with hot glue. Measurements were performed at room temperature (25 ± 1 °C) and at reduced pressure (<0.2 mbar). The sample-detector distance was 550 mm for the polymer solutions, whereas acquisitions at distances of both 2500 mm and 262 mm were performed for the NPs in water samples. The available q range was therefore 0.1–6.0 nm^{-1} and 0.042–17 nm^{-1}, respectively. The two-dimensional scattering patterns were subtracted for the "dark" counts, and then masked, azimuthally averaged, and normalized for transmitted beam intensity, exposure time, and subtended solid angle per pixel, by using the FoxTrot software developed at SOLEIL. The one-dimensional intensity vs. q profiles were subtracted for the contributions of the empty capillary and the solvent (acetone or water) and put in intensity units of macroscopic scattering cross-section (cm^{-1}) by dividing for the capillary thickness estimated from the alignment scans. Model calculations of scattering profiles were performed using the software SasView (SasView version 5.0.2, (n.d.). https://www.sasview.org/ (accessed September 7, 2019)) and SASfit.[38] In order to get an indication of the size in the real space of the inhomogeneities giving rise to the SAXS profiles, pair distance distribution functions were obtained by indirect Fourier inversion using the software GNOM of the ATSAS package.[39]

2.2.11. Poly(di)glycerol adipate and Poly(di)glycerol adipate-hexanediol synthesis

PGA and P(D)GAHex were synthesised via enzymatic polymerisation of divinyl adipate (DVA) and (di)glycerol following the published protocol of Jacob *et al.* [28].

For PGA synthesis, (di)glycerol (12.50 mmol) and DVA (12.50 mmol) were weighed into a 20 mL glass vial and dissolved in THF (10 mL). Novozym 435 (0.11 g) was added to the mixture which was then stirred at 200 rpm at 50 °C for 5 h in a sealed vial. The rubber septum was pierced with a needle to allow the release of acetaldehyde, a by-product of the reaction. After 5 h, the reaction was stopped by removal of the enzyme by filtration. The solvent was removed under reduced pressure. The polymer was kept under reduced pressure at 25 °C for at least 3 days to removed residual solvent leaving a viscous, pale-yellow polymer. The polymer conversion was quantitative, as confirmed by ^{1}H NMR spectroscopy. The polymers were not further purified.[24,27]

For P(D)GAHex synthesis, 1,6-n-hexanediol (6.25 mmol), (di)glycerol (6.25 mmol) and DVA (12.50 mmol) were weighed into a 20 mL glass vial and dissolved in THF (10 mL). Novozym 435 (0.11 g) was added to the mixture and the following steps were performed as described above.

2.2.12. NPs formulation

NPs were prepared by nanoprecipitation following the method published by Taresco *et al.* [30].

Polymer (10 mg) was dissolved in acetone (2 mL) and then added dropwise into deionised water (4 mL) under constant stirring at 500 rpm. The uncapped solutions were left stirring overnight to allow for complete evaporation of acetone. The final NPs concentration was 2.5 mg/mL.

2.2.13. Coumarin encapsulation study

Coumarin (coumarin6 (Cou6) or 6,7-dihydroxy-4-methylcoumarin (MeCou)) solutions (2 mg/mL) were prepared in acetone. Polymer (10 mg) was weighed into a vial and dissolved in coumarin solution (2 mL). Polymer solutions were subsequently added dropwise into deionised water (4 mL) whilst stirring at 500 rpm. Vials were left under stirring overnight to enable acetone evaporation. Nanoparticle-dye dispersions were filtered through a 0.22 μm filter. Coumarin blank was filtered and measured in water without the addition of polymer. Encapsulation was determined

using UV–vis spectrophotometry and particle sizes and Z-potential were determined using DLS.

2.2.14. NPs stability in BSA (low and high concentration)

Stock solutions of PGA, PDGA, PGAHex, and PDGAHex were prepared at 2 mg/mL. Stock solution of bovine serum albumin (BSA) was prepared at 0.2 mg/mL in DI water. PGA, PDGA, PGAHex, and PDGAHex (900 μL) were mixed with BSA (100 μL) in different vials. The mixtures of NPs and BSA were incubated for 24 h. Samples were measured in DLS at t = 0, 3 and 24 h to assess the stability of NPs in BSA.

PGA and PDGA showed low stability when treated with 0.2 mg/mL, while PGAHex and PDGAHex were relatively stable in this condition. Therefore, further stability studies were conducted, on PGAHex and PDGAHex, in more concentrated solution of BSA (2 mg/mL) in DI water. NPs (150 μL) and BSA (150 μL) were mixed (resulting in NPs concentration of 1 mg/mL and BSA concentration 1 mg/mL), and samples were analysed by DLS to assess the stability of the NPs at the given time intervals.

2.2.15. ΔA% calculation

The absorbance of the NPs-dye dispersions was measured using a UV–vis spectrophotometer multi-well plate reader at λ_{max} = 440-nm. The apparent solubility (ΔA%) of each formulation was determined using equation (1), previously developed by Sanna *et al.* [40]

$$\Delta A\% = \frac{\Delta A}{A_0} \times 100 = \frac{(A - A_0)}{A_0} \times 100 \qquad (1)$$

2.2.16. Cytotoxicity of polymer NPs in vitro

HCT116 human carcinoma colon epithelial cells were purchased from the American Type Culture Collection (ATCC). Cells were cultured in Dulbecco's Modified Eagle Medium (DMEM) supplied with 10% (v/v) Fetal Bovine Serum (FBS), and 2 mM L-glutamine at 37 °C with 5% CO$_2$. The PrestoBlue cell viability assay (Thermo Fisher Scientific) was performed to assess NP cytotoxicity via the measurement of cellular metabolic activity. Cells were seeded at 1×10^4 cells/well in 96 well plates and cultured for 24 h prior to assaying. Formulations were exposed to cells at a concentration 0.5 mg/mL for 48 h and applied in 100 μL phenol red free DMEM containing 10% (v/v) FBS. Following exposure, formulations were removed and 100 μL of 10% (v/v) PrestoBlue reagent diluted in a phenol red free medium was applied per well for 30 min. The resulting fluorescence was measured at 560/600 nm ($\lambda_{ex}/\lambda_{em}$). Relative metabolic activity was calculated by setting values from the negative control as 100% metabolic activity.

2.2.17. Cytotoxicity and uptake of polymer NPs in vivo

The cytotoxicity of polymers was investigated by challenging *Caenorhabditis elegans* nematodes to polymers PGA, PGAHex, PDGA and PDGAHex (0.5 mg/mL). Briefly, *C. elegans*, maintained on nematode growth media agar, were synchronised (eggs, Day 1, 20 °C) and collected (adults Day 4, 20 °C) using M9 Buffer. [41] Adult *C. elegans* were filtered (Merk 20 μm Nylon filter) and washed with M9 buffer solution (50 mL). *C. elegans* was collected and counted and made up 10–20 nematodes in 0.5 mg/mL of polymer, suspended in M9 buffer solution, with 0.1 OD$_{600}$ of *Escherichia coli* for sustenance. Controls were used for experimental guidance in the form *E. coli* alone (positive control) and absolute ethanol (20% v/v, negative control). Nematodes were imaged at Time = 0 h upon addition of challenge and at Time = 24 h. All experimental conditions were conducted in triplicate with a minimum of 10 nematodes per challenge. Viability of nematodes was determined according to motile percentage calculations. [42] An absolute indicator of nematode viability was also determined through the observation of progeny production after 24 h.

NGM agar plates containing synchronized cycles of *C. elegans* (L4-young adult stages) were harvested using sterile ultra-pure deionised water (18.2MΩ). The nematodes were washed with sterile deionised water (1 mL, 3 times) and collected using centrifugation (2500 rpm, 1 min). *C. elegans* (∼300 nematodes) were dosed with PGAHHex and PDGAHex nanoparticles at 0.5 mg/mL (n = 3) for 24 h and washed prior to imaging (3 times, 5 mL of sterile deionized water, centrifugation 1500 rpm,1 min). Regions of interest containing *C. elegans* that had ingested fluorescent nanoparticles were imaged using Eclipse T1 and QIMAGING optiMOS camera equipped with CoolLED pE-4000 fluorescence illumination and pE-100 brightfield illumination and Nikon Plan Fluor 10 × (0.30NA) objective. Pictures analysis details in table below (Brightfield: 5 ms, Green: 300 ms).

	Lower Threshold	Upper Threshold
Control	180	200
PGA	180	200
PGDGA	180	1400

3. Results & discussion

3.1. Synthesis of PGA and PDGA

PDGA and PGA successful enzymatic synthesis in THF (Scheme 1) was confirmed by different analytical and spectroscopical techniques. The synthesis of PGA has been previously reported in the 'greener' 2-MeTHF, [28] however, diglycerol was found to be insoluble in 2-MeTHF, preventing the polymerisation from proceeding.

^{1}H NMR spectroscopy confirmed the consumption of DVA vinyl protons in both PGA polymers (Fig. 1A-B and S1). Peaks at 7.26, 4.83 and 4.55 ppm, indicative of the vinyl group of DVA were found not to be visible in the ^{1}H NMR spectrum of PGA. Differently, traces of vinyl protons could be seen in the ^{1}H NMR spectra of PDGA polymers (Fig. 1C and S2). This may be explained by the lower molecular weight observed in the PDGA polymerisation, resulting in a higher concentration of vinyl polymer end groups per sample compared to PGA. Additionally, the expected chemical shift from 4.0 to 4.26 ppm of the glyceryl protons was observed in the ^{1}H NMR spectrum of PGA.[24] While, in the ^{1}H NMR spectrum of PDGA, a broadening of the –CH_2 proton peak, attributed to the ether adjacent protons of diglycerol, was observed at 3.56 ppm. A shift from 3.56 ppm to 4.13 ppm was observed for the ester adjacent –CH_2 protons, a downfield shift indicative of successful esterification. Moreover, a broad peak at 3.97 ppm was confirmed to be that of the methine proton of the 1,2-disubstituted diglycerol group.[24]

In accordance with previous ^{1}H NMR literature on PGA,[24,28] broadening of the adipate protons at 1.66 and 2.39 ppm was seen in both polymers, indicating successful polymerisation of DVA into a polymeric species, PGA and in this new example PDGA. The peak

at 5.30 ppm in the ^{1}H NMR spectrum of PGA indicates low levels of branching, *ca.* 10%, (1,2,3-trisubstitution of the glyceryl group) giving further evidence of successful polymerisation of predominantly linear motif.

A peak at 5.02 ppm in the ^{1}H NMR spectrum of PDGA, indicative of 1,2,3-trisubsitution of the diglyceryl group was observed. The level of 1,2,3-trisubstitution of PDGA was determined to be *ca.* 6% (integral of peak at 5.02 ppm, with respect to CH$_2$ adipate proton peak at 1.66 ppm). The presence of a methine proton in this position was confirmed by HSQC ^{1}H NMR spectroscopy (**Figure S3**). The likelihood of a reaction at the secondary hydroxyl position of both glycerol and diglycerol remains low due to the regioselectivity of the enzyme. [43] The lower levels of branching in PDGA may be a result of additional steric hindrance at the secondary hydroxyl position of diglycerol, further reducing the likelihood of reaction at the site.

### 3.2. Synthesis of modified PGA and PDGA

Following the successful synthesis of both PGA and PDGA, 1,6-*n*-hexanediol was added in stoichiometric amount with the aim of synthesising PGA and PDGA derived polyesters with a variation in their hydrophilic-hydrophobic balance (Scheme 2).

The successful incorporation of 1,6-hexanediol (Hex) was confirmed by ^{1}H NMR spectroscopy (Fig. 2, **S4 and S5**). A shift in the peak of the internal chain –CH$_2$ protons of Hex from 1.37 to 1.41 ppm was observed. This peak was also found to be broadened, both indicative of successful polymerisation. The peak of –CH$_2$ (yellow protons, Fig. 2, **S4 and S5**) also shifted from 1.52 to 1.65 ppm in agreement with results previously published by Jacob *et al.* [28] Post polymerisation, this peak lies in the same region as the adipic protons of both PGA and PDGA. No residual –CH$_2$ proton peak could be seen at 1.52 ppm indicating complete incorporation of Hex into the polymer backbone. A shift in the alcohol/ester adjacent –CH$_2$ proton peak of hexanediol from 3.54 to 4.07 ppm was also observed, further confirming the incorporation of Hex into the polymer backbone.

As was seen with the ^{1}H NMR analysis of unmodified PGA and PDGA, peak broadening of the adipic –CH$_2$ protons at 1.66 and 2.39 ppm was observed, although the latter now coincides with –CH$_2$ protons of Hex (orange protons, Fig. 2, **S4 and S5**). A lower level of 1,2,3-trisubstitution (∼4%) was seen in the ^{1}H NMR of PGA-Hex, as previously reported by Jacob *et al.* [28], likely due to the lower concentration of secondary hydroxyl groups available to participate in the reaction. This phenomenon was also observed for the PDGAHex modification where the level of 1,2,3-trisubstitution lies around 4% with a minor peak at 5.02 ppm in the ^{1}H NMR spectrum.

3.3. Molecular weight analysis in organic solvent

GPC analysis confirmed the successful polymerisation of both PGA and PDGA. The molecular weight of PDGA was found to be slightly lower than that of PGA with varying dispersity values for
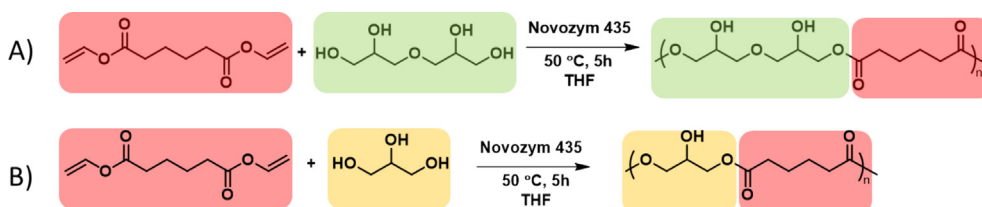
Scheme 1. Enzymatic synthesis of A) PDGA, B) PGA in THF. Only linear polymer representations have been shown due to the low levels of 1,2,3-trisubstitution within the polymer as a result of the regioselectivity of the enzyme.[24,43].
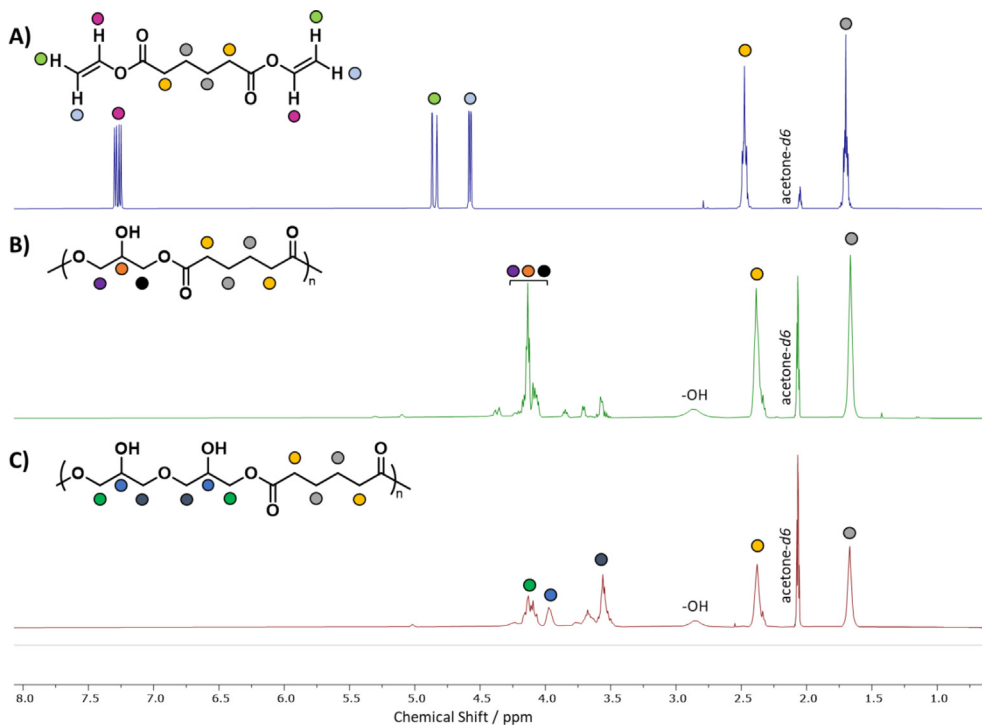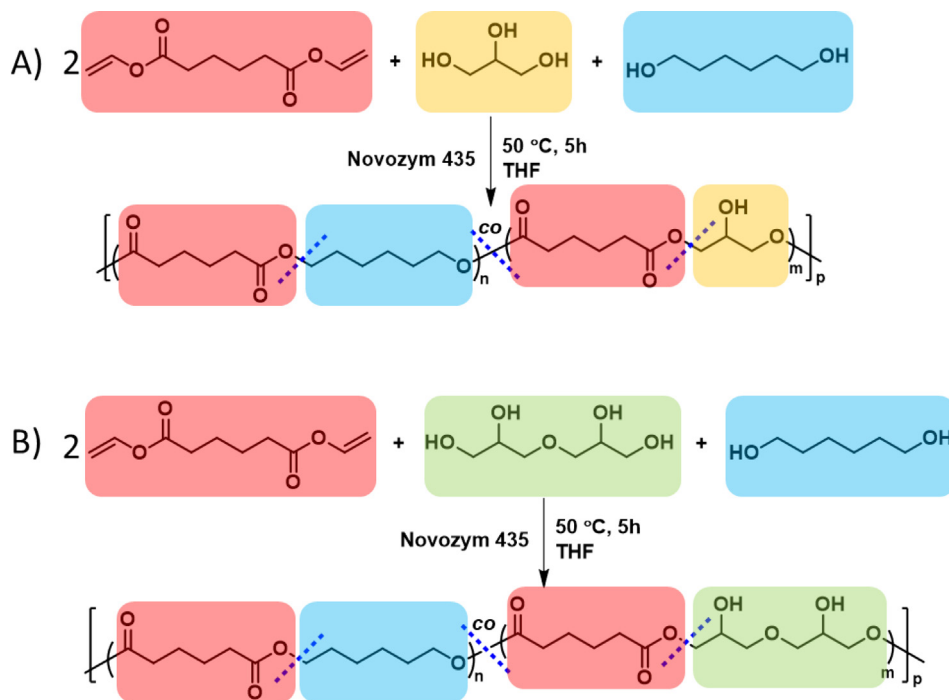
Fig. 1. ^{1}H NMR spectra of A) DVA B) PGA C) PDGA. Peaks between 3.5 and 4.0 ppm in spectra B and C are the result of polymer end group protons which have been described in more depth in **Figures S1 and S2**.

Scheme 2. Enzymatic synthesis of A) PGAHex and B) PDGAHex in THF. Only linear representations of PGAHex and PDGAHex have been included due to the low levels of 1,2,3-trisubstitution of (di)glycerol in the polymer backbone, a result of the regioselectivity of the enzyme.[43] The degree of 1,2,3-trisubstitution observed in PGAHex and PDGAHex was further reduced compared to unmodified PGA and PDGA due to the reduced amount of glycerol, and consequently the lower concentration of secondary hydroxyl groups available to react.[24,28] Blue dashed lines indicate that the diols in the polyester backbones may not be ideally alternating.

both polymers (PGA (2.6) and PDGA (1.7)) (Table 1, Entries 1 and 2; chromatogram traces in **Figure S6** left). This finding is consistent with the higher concentration of vinyl protons seen in the ^{1}H NMR spectrum of PDGA, suggesting that there is a higher concentration of polymer vinyl chain ends as a result of the shorter chain

length of PDGA. The lower molecular weight of PDGA can be explained by the increased viscosity of diglycerol compared to glycerol, reducing the ability of the monomers and enzyme to mix and react in more viscous conditions. The molecular weights of the modified polymers were found to be higher than those with
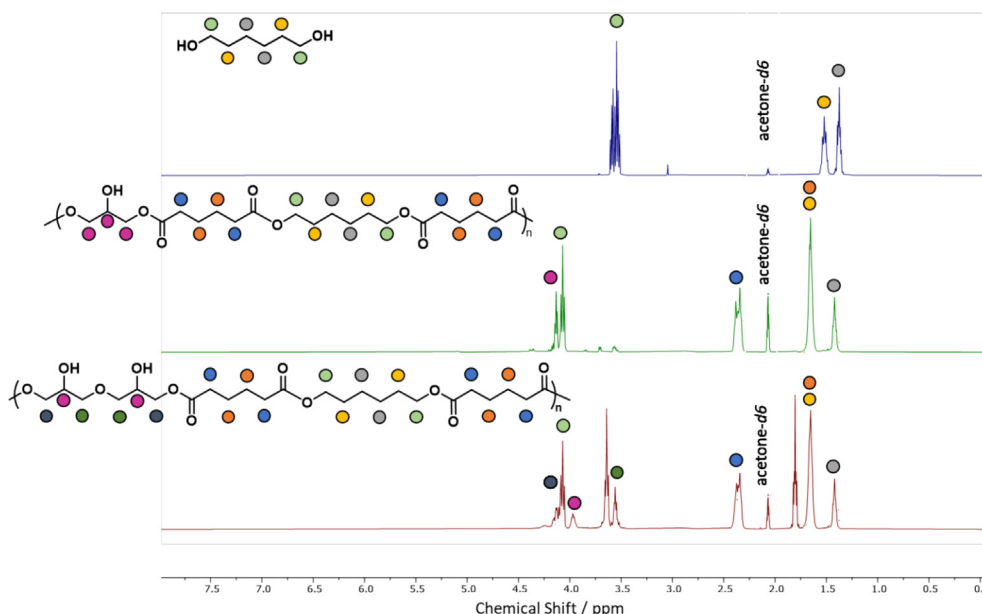
Fig. 2. ^{1}H NMR spectra of A) Hexanediol, B) PGA-hex, C) PDGAHex. The structures of the polyester backbones have been simplified for clarity. However, the (di)glycerol and hexanediol may not alternate in an ideal fashion as has been depicted here.

Table 1
Number average molecular weight (M_n), dispersity (Đ).

Entry	Sample	M_n / g mol^{-1} [a*]	Đ[a]	T_g / °C[b]	Θ_w / °
1	PGA	4930	2.6	−29	58.8 ± 1.1
2	PDGA	3220	1.7	−20	44.0 ± 1.0
3	PGAHex	6250	2.0	−48 (T_m = 8)	63.3 ± 0.5
4	PDGAHex	7450	2.1	−37	55.5 ± 1.3

[*] Polymers were not further purified post polymerisation; therefore, oligomeric peaks are visible in GPC and were taken into account during polymer analysis.
[a] Molecular weight was determined by GPC using THF eluent at 40 °C. GPC was calibrated using PMMA standards with molecular weight ranging from 540 to 1.02 × 10^6 g mol^{-1} and dispersity (Đ) of approximately 1.
[b] Thermal properties determined by DSC.

unmodified backbones (Table 1, Entries 3 and 4; chromatogram traces in **Figure S6** right). This is possibly due to the increased solubility of hexanediol in THF in comparison to glycerol, resulting in a higher propensity for hexanediol to react compared to the glycerol/diglycerol alone, driving up the molecular weight of the polymers.

3.4. Analysis of water-soluble chains

Since polymers were characterised and used for chemical, physical and biological characterisations without any post polymerisation purification steps, it was possible to notice oligomeric peaks in all the GPC traces. Although this is aligned with the manipulation processes previously reported in the literature of PGA, in the present work, we were also interested in understanding whether the short chains would show a different solubility behaviour. Considering the low molecular weight observed in the GPC traces, it was hypothesised that these were water soluble, therefore, AUC-SE analysis in aqueous environment was performed. AUC-SE measured molar mass information on the aqueous-soluble fraction based on its interaction with the centrifugal field were obtained by measuring concentration (in interference fringe displacement units) as a function of radius. PGA and PDGA were more soluble than their hexanediol equivalents, with 50–100 fringe increments compared to ∼ 10 fringe increments, respectively. Assuming a refractive index increment of 0.13 mL/g, [44] this is equivalent to 2–4 % and 0.4 %, compared to the theoretical 10 % in preparation.

PGA measured at 600 Da (rmsd 0.017), PGDA measured at 1400 Da (rmsd 0.054), PGAHex at 900 Da (rmsd 0.0067) and PGDA-Hex at 500 Da (rmsd 0.0069) (**Figure S7**). Polydispersity indices, based off z-average/w-average molar mass, were all 1.8 with the exception of PGA which was 2.2. The knowledge of the solubility tendency of the short oligomers may be exploited in formulations in which water-soluble carriers are needed and considering the flexibility of the synthetic approach adopted here, short chains can be easily accessed.

3.5. Physical properties

All polymers, with the exception of PGAHex, were found to be amorphous with T_gs below −20 °C (Table 1 **and Figure S8–11**). The T_gs of PGAHex and PDGAHex were lower than those seen in the bare polymers. This may be a result of the higher flexibility introduced by Hex in comparison to the unmodified PGA and PDGA (Table 1). The reduction in hydrogen bonding between chains as a result of the introduction of Hex and the consequent decrease in fraction of glycerol/diglycerol could also explain the decrease in T_g for the modified polymers (Table 1). In addition to this, the increased hydrogen bonding in PDGA, as a result of the additional pendant hydroxyl group may explain their higher T_g compared to PGA. [45,46].

A weak endothermic band was observed with PGA-Hex (**Figure S10**), in agreement with previously reported results, possibly related to melting of crystalline portions, induced by increased

symmetry caused by the addition of the hexanediol chain. [28] No melting transition band was observed for PDGAHex, likely because the additional glycerol group disrupts the symmetry observed instead for PGAHex.

Water contact angle (Θ_w) measurements were taken to determine the wettability of the polymer films. Θ_w of PDGA (44.0 ± 1.0) was found to be lower than that of PGA (58.8 ± 1.1), reasonably because of the larger fraction of the hydrophilic polyol segments in the diglycerol containing polymer compared to the glycerol containing one (Entries 1 and 2, Table 1). The same trend was observed with PGAHex (63.3 ± 0.5) and PDGAHex (55.5 ± 1.3) (Entries 3 and 4, Table 1). The water contact angles of the hexanediol modified polymers were found to be higher than those of the unmodified polymers, indicative of a lower overall hydrophilicity of the polymer upon inclusion of hexanediol in its chain.

Rheological shear ramp experiments were conducted to gain insight into the flow behaviours of the synthesised materials (Fig. 3). A similar pattern could be observed for all the polymers where at relatively low shear rates Newtonian (constant viscosity regardless of shear) behaviour was observed. Once a critical shear rate was exceeded, rapid shear thinning was measured, producing a typical example of a non-Newtonian shear thinning material. [47] The critical shear rate is dependent on the force required to overcome intermolecular interactions and to align and disentangle polymer chains in the direction of the applied force. Polymers with longer and more entangled polymer chains, or with greater intermolecular interactions (i.e. through increased hydrogen bonding between chains) are therefore expected to display a higher critical shear rate. In our case, PDGA and PGA display the highest critical shear, reasonably because of a significantly larger amount of hydrogen bonding between polymer chains in comparison to PDGAHex and PGAHex.

The combination of chemical and physical characterisations allowed us to both confirm the successful polymerisations and investigate the key properties of these novel library of functional and amphiphilic polyesters. It was clear how the addition of the extra hydroxyl group of the diglycerol moiety enabled the formation of more hydrophilic chains but at the same time more hydrogen bonding centres. The stoichiometric combination of a polyol and a hydrophobic/flexible diol permitted the fine tuning of thermal, rheological and wettability features. Gathering this information facilitates a more in depth understanding of the behaviour of the NPs derived from these materials and their possible application as enhanced carriers in drug delivery.

3.6. Polymer self-assembly

The amphiphilic balance of the starting scaffold PGA was adjusted by incorporating first 1,6-n-hexanediol, as from previous literature, [28] then diglycerol and finally both. The change in the hydrophilic/hydrophobic nature of the polymers was confirmed by water contact angle measurements as well as by the self-assembly of the polymers in aqueous environment. The polymers were nanoprecipitated into deionised water, providing NPs with sizes ranging from 120 up to 150 nm with very low PDI values (between 0.02 and 0.2) (Table 2). Switching from glycerol to diglycerol led to an increase in the hydrodynamic size of the polymer NPs, most likely due to the increase in hydrophilicity of the aggregated structures. While the addition of 1,6-hexane diol led to a decrease in the size of the NPs of both PGAHex and PDGAHex compared to the unmodified polymers. The observed trends suggest that the smaller NPs size may be a result of nanoaggregates with more tightly assembled polymer chains. This is expected to occur in polymers with higher degrees of hydrophobicity.

The obtained sizes were also verified by TEM analysis, showing spherical nanoaggregates with an average diameter of between 98 and 157 nm (**Figures S12-15 and S19**). The sizes are generally in good agreement with those inferred by DLS. Generally, throughout the samples some shrinkage was observed, induced by the dehydration that the samples undergo during the preparation for the measurements. In additon, some aggregation was also seen, in particular, for the PDGAHex sample, which may be likely due to sample preparation non-optimisation. These phenoma may justify the slightly different avarage sizes obtained with TEM when comepared to the hydrated sample *via* DLS. [48]

3.7. NPs stability

Many conventional nanoformulations require the addition of stabilisers or surfactants in order to achieve stability. [49] We observed stable dispersions of all the NPs produced in the present work, without the addition of any additional stabilisers or surfactants, at a concentration of 2.5 mg/mL. For all the samples, a negative zeta-potential was obtained, suggesting that the formed NPs are well dispersed in water because of good electrostatic repulsion. As for PEGylated NPs, the zeta potentials of our NPs were negative. This is likely due to the presence of a hydrophilic shell due to the presence of free hydroxyl groups and the corresponding association of anions to form the outer layers as in case the oxyethylene units in PEG coronas. [50,51] The zeta-potential of the PDGA based polymer NPs is significantly lower than that of the PGA based NPs (Table 2). This can be attributed to the extra pendant hydroxyl groups in the PDGA facilitating additional interactions of the polymeric nanoaggregates with water. In all the cases, an additive effect due to the possible presence of carboxylic end groups may also be in action.

In agreement with the zeta-potential measurements, polymer NPs were found to be generally stable in biological conditions, using bovine serum albumin (BSA) as a model protein.[52,53] NPs of PGA, PDGA, PGAHex, and PDGAHex at 1.8 mg/mL were incubated with 0.2 mg/mL BSA for 24 h at 37 °C, and their sizes were measured at predetermined times by DLS. PGA and PDGA NPs became larger over time when treated with BSA (Table 3). However, particle sizes of PGAHex and PDGAHex tended to increase very slightly or even remain unchanged at three different time points. PDGAHex appears to be the most stable of the hexanediol modified polymers, due to the presence of abundant hydrophilic ether groups and pendant hydroxyl functionalities that facilitate the formation of a stable hydration shell and the dispersion in aqueous media. The hydration shell creates an efficient steric hindrance to the formation of aggregates with BSA, which in turn makes the PDGA-Hex NPs more resistant and stable upon addition of this protein. Protein binding assay using BSA is also influenced by the solution pH. Indeed, since the isoelectric point (IEP) of albumin is at pH 4.7, BSA is negatively charged above the IEP.[54]
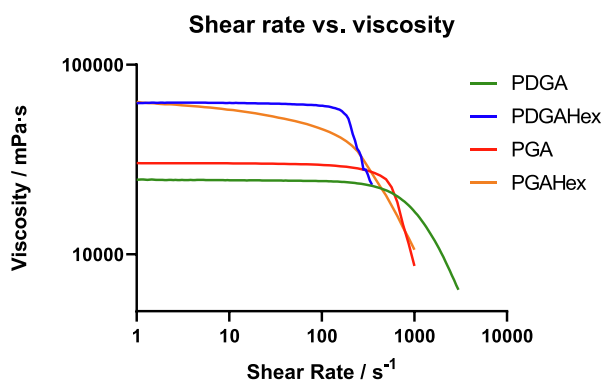

Shear rate vs. viscosity

Fig. 3. Rheology of PGA, PDGA and hexanediol modifications.

Table 2
Size, PDI and zeta-potential of PGA and PDGA NPs.

Entry	Sample	Average size / nm[a]	PDI[a]	Zeta potential / mV
1	PGA	138.2 ± 0.4	0.02 ± 0.01	−12.8 ± 0.3
2	PDGA	150.2 ± 0.7	0.07 ± 0.02	−21.9 ± 0.9
3	PGAHex	120.2 ± 1.3	0.05 ± 0.03	−12.6 ± 0.7
4	PDGAHex	140.1 ± 1.6	0.21 ± 0.02	−29.0 ± 0.4

[a] Data acquired by DLS measurements.

Table 3
Stability of polymer nanoparticles against BSA (0.2 mg/mL) after 0, 3 and 24 h.

Entry	Sample	Time / h	Size / nm[a]	CAC (µg/mL)
1	PGA	0	279.3 ± 10.7	170
2		3	353.0 ± 13.7	
3		24	400.0 ± 4.0	
4	PDGA	0	268.4 ± 2.0	240
5		3	412.6 ± 20.0	
6		24	501.2 ± 144.2	
7	PGAHex	0	203.8 ± 7.0	180
8		3	244 ± 8.0	
9		24	261.9 ± 2.2	
10	PDGAHex	0	139.0 ± 5.0	80
11		3	139.6 ± 5.3	
12		24	135.3 ± 1.0	

[a] Size determined by DLS.

Moreover, the net charge of the BSA at pH 7 was found to be −18 mV, so the higher the negative surface charge of the NPs, the higher the electrostatic repulsion within BSA and NPs. This confirms better stability of the PDGAHex NPs compared to PGA-Hex. Building on this, the stability of the more stable formulations, PGAHex and PDGAHex was screened again in the presence of BSA, at concentrations comparable to physiological conditions.[53] The size of the NPs was observed to remain largely unchanged after exposure to the higher concentration of BSA after 24 h (181.8 and 136.5 nm for PGAHex and PDGAHex respectively, Table 4, entries 3 and 6 and **Figure S17**).

Furthermore, the thermodynamic stability of the NPs was quantified using critical aggregation concentration (CAC) measurements by DLS (Table 3 **and Figure S18**). It was found that NPs of PDGAHex have the lowest CAC value (80 µg/mL) (**Figure S18**) suggesting that PDGAHex has a greater propensity to self-assemble in water. The techniques used to assess the stability of the NPs are in good agreement throughout the library of polymers.

3.8. SAXS analysis of polymers and related NPs

SAXS analysis was first performed on the unformulated polymers to determine their behaviour and arrangement in acetone (the solvent from which the nanoformulations were prepared). The SAXS analysis of the synthesized polymers solubilized in acetone, at a concentration of 10 mg/mL (Fig. 4 and **Table S2**), follow a similar trend as the findings summarized in Table 1. The experi-

Table 4
Stability of polymer NPs against BSA (high concentration from Methods) after 0, 3 and 24 h.

Entry	Sample	Time / h	Size / nm[a]	PDI[a]
1	PGAHex	0	184.2 ± 5.3	0.11 ± 0.02
2		3	183.6 ± 3.9	0.09 ± 0.02
3		24	181.8 ± 0.4	0.08 ± 0.01
4	PDGAHex	0	141.2 ± 0.1	0.05 ± 0.01
5		3	139.8 ± 2.4	0.07 ± 0.02
6		24	136.5 ± 1.6	0.06 ± 0.01

[a] Determined by DLS.

mental scattering profiles were interpreted according to the model of polydisperse flexible polymers with Gaussian statistics.[55,56] The M_n and Đ values were fixed to those found by GPC analysis (although different organic solvents were used), whereas the radius of gyration (R_g) and the intensity extrapolated at zero angle ($I(0)$) were optimized to fit the data. From the $I(0)$ value on absolute scale, the polymer partial density (d) in solution that had to be assumed to agree with the known mass concentration of the samples was also estimated (see SI, R_g and d values reported in Fig. 4). The average size of the modified polymers containing Hex were found to be indeed larger compared to the unmodified PGA and PDGA polymers, as also seen from the pair distance distribution functions that extend to larger maximum dimensions above 7 nm. The power law followed by the scattering profiles in the high q range (>1 nm^{-1}) was satisfyingly reproduced by the Gaussian coil model, suggesting that the polymers in acetone at 25 °C do not appreciably deviate from the θ-solvent conditions. In the case of PGAHex (Fig. 4C), a clear intensity upturn in the q range < 0.3 nm^{-1} deviating from the expected profile for the individual polymer coil (dashed black line) was detected. In this case the data could be reproduced by assuming an additional contribution from spherical large aggregates (average diameter of the order of 100 nm, grey dashed line), that, if the same density of the polymer is assumed, would contribute for<4 % of the dispersed polymer mass. Considering that PGAHex is the least polar of the series (with the largest water contact angle, see Table 2), it could be that a small fraction with highest molecular weight has some tendency to aggregate in acetone.

The SAXS profiles collected on the water suspensions of the nanoprecipitated polymers are in agreement with the average diameters determined by DLS and TEM analyses. Due to the minimum q being 0.045 nm^{-1} (corresponding to a maximum detectable size of $\pi/0.04 = 75$ nm), the scattering signal from the particles is for great part beyond the accessible q range. The recorded profile shows a characteristic slope related to the particle-solvent sharp interface observed in the q range 0.08–0.2 nm^{-1} (q^{-4} according to the Porod law), before the signal starts to fall into noise level. Nevertheless, reasonable P(r) functions could be estimated imposing maximum sizes coincident with the average diameters obtained by DLS (Fig. 5, **inset**). The absence of evident oscillations
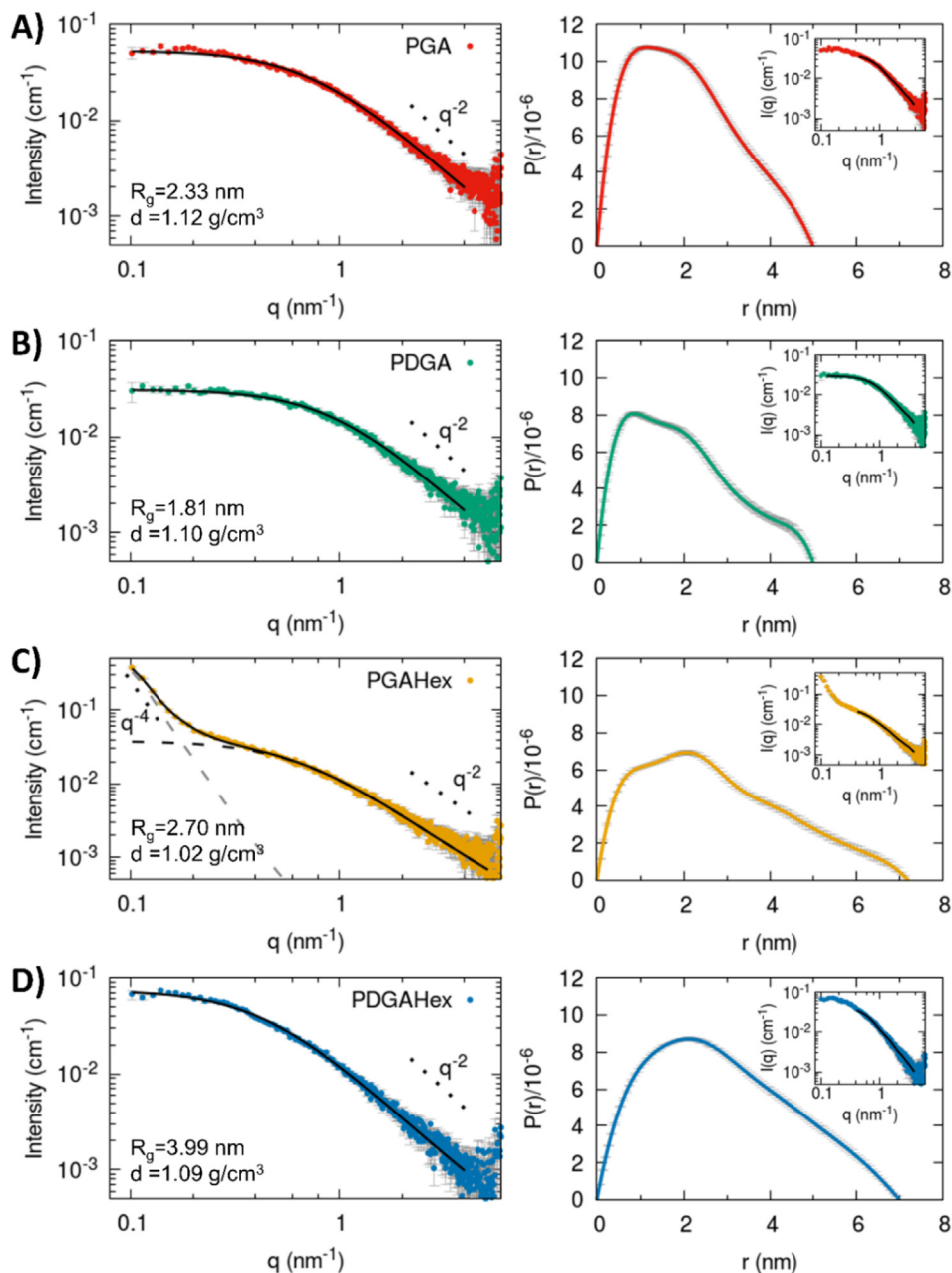
Fig. 4. SAXS analysis of the polymers PGA (A), PDGA (B), PGAHex (C) and PDGAHex(D) dissolved in acetone at 10 mg/mL. On the left: experimental scattering profiles on absolute scale (coloured dots) and calculated theoretical profiles (black line) according to the model of polydisperse Gaussian coil. On the right, pair distance distribution functions P(r) obtained by indirect Fourier inversion. The corresponding fits to the data in the q-range considered are shown in the insets.

due to a spherical form factor suggests rather high size polydispersity, in agreement with TEM analysis. The preparation protocol has a different impact on the final concentration of particles for the four polymers: a higher number density can be inferred for PDGA-Hex NPs considering that the detected signal is one order of magnitude higher than for nanoprecipitated (and filtered) PGA and PGAHex NPs; in the case of PDGA no appreciable signal from the NPs could be detected in the final sample. For this latter we could speculate that the particle concentration had been decreased below detection limit due to both filtration of larger particles and higher solubility in water.

3.9. NPs cytotoxicity

Both PGA and PGAHex have previously been shown to be promising materials for drug delivery after showing minimal

cytotoxicity against a NIH 3 T3 cell line. [28] The cytocompatibility of PGA, PDGA, PGAHex and PDGAHex NPs, prepared with acetone, were assessed at a polymer concentration of 0.5 mg/mL against the HCT116 intestinal epithelial cells (Fig. 6A). Cell viability exceeded 93% for all formulations following 48 h incubation, indicating that the NP formulations are non-toxic which is in agreement with previously published data. Furthermore, the in vivo cytotoxicity of the polymer NPs was assessed (Fig. 6B).

3.10. Whole organism viability

All NPs did not exhibit significant changes in C. elegans viability, measured as a function of nematode viability, after 24 h of exposure ($p > 0.05$, Fig. 6B). This was observed by comparable nematode motility between unchallenged control and polymer treated C. elegans, as well as the production of progeny over the 24 h
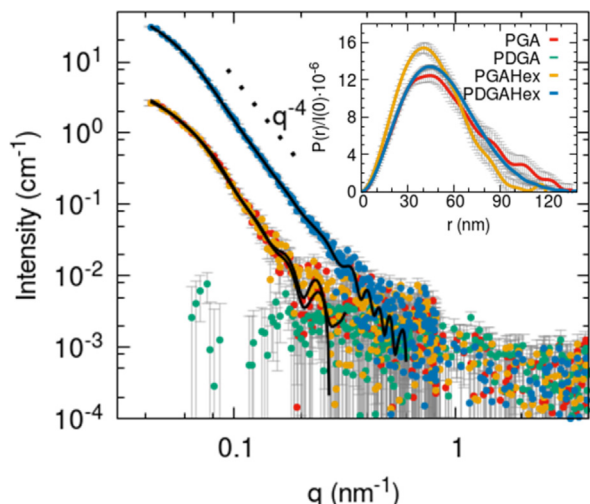
Fig. 5. Experimental SAXS profiles of the nanoprecipitated polymers in aqueous solution (expected concentration 2.5 mg/mL). The P(r) functions are shown in the inset, and the corresponding fits are shown as black lines superimposed to the experimental data.

experimental challenge (Fig. 6C **and Supplementary video**). Polymers PGAHex and PDGAHex appear to aggregate after 24 h when suspended in M9 buffer solution, nonetheless no toxicity effect was observed. Nematodes were observed feeding on aggregates, which also did not affect nematode viability. Nematodes challenged with absolute ethanol (20% v/v) displayed, an immediate

decrease in viability and motility upon challenge initiation. Nematodes challenged with ethanol also did not exhibit the production of progeny throughout the experiment, further indicating the absence of viability. Therefore, all the polymers appear to demonstrate *in vivo* biocompatibility, validating these polymers as a suitable tool to deliver to whole organism systems, as well as nematodes serving as a suitable organism to evaluate the efficacy of novel drug delivery tools. [57].

3.11. Encapsulation study

The ability of the polymer NPs to encapsulate hydrophobic and amphiphilic compounds was assessed by co-nanoprecipitation of the polymer with coumarin 6 (Cou6) (XLogP3 = 4.9) [58] and MeCou (XLogP3 = 1.5) [59]. Cou6 has previously been used in encapsulation studies as a model hydrophobic compound with a drug-like structure. [60,61] It is highly insoluble in water, similar to many pharmaceutical compounds while MeCou shows a higher water solubility. In Table 5, size, PDI and zeta potential of Cou6 loaded polymer NPs are reported, while in Fig. 7A and 7B the DLS profiles are shown.

The apparent solubility of each drug in water was determined in a fast and semi-quantitavie fashion by using ΔA%. The polymers were then ranked according to their ΔA% value, indicative of an apparent solubility enhancement of Cou6. [28] PGA and PDGA showed lower ΔA% values compared to their hexanediol modified counterparts (1500 and 500 vs 2500 and 10,000 respectively) (Fig. 7C). The increase in apparent solubility of Cou6 in the PGAHex and PDGAHex formulations can be attributed to an improvement in the amphiphilic balance by the introduction of hexanediol into
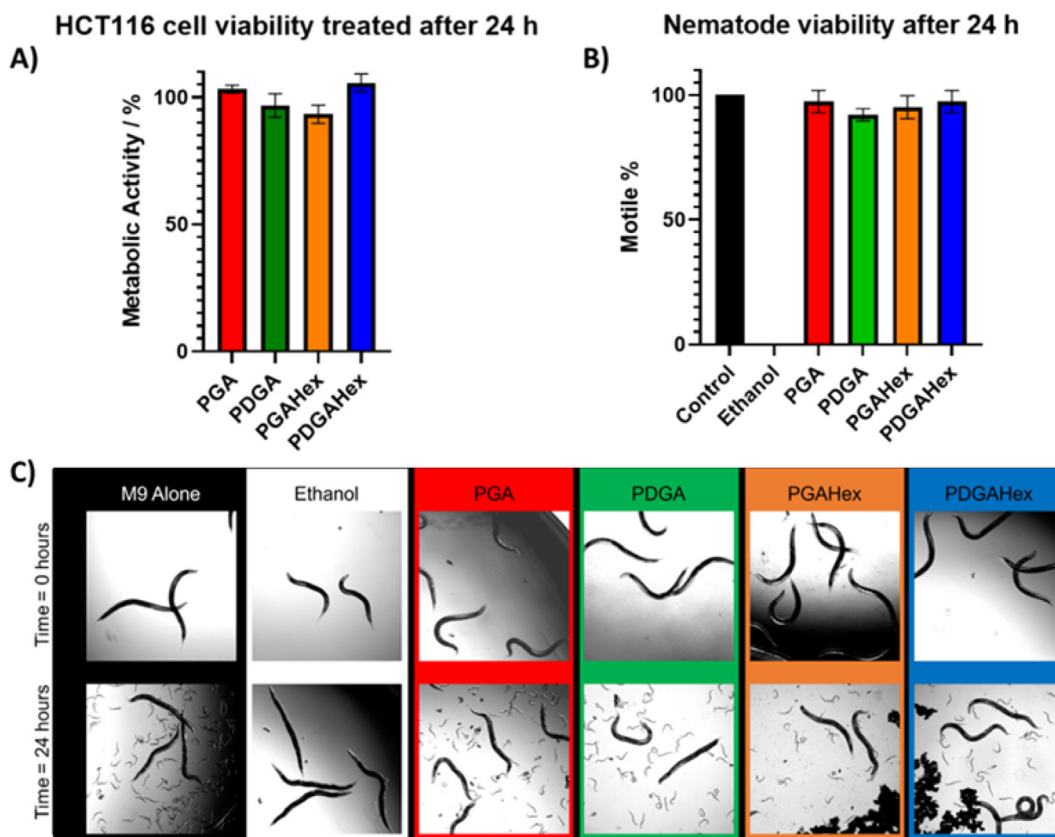

Fig. 6. A) Cell viability after 48 h, tested on HCT116 human carcinoma colon epithelial cells. **B)** *C. elegans* viability, as a function of motility, after completion of 24 h challenge with polymers; experiments were conducted in triplicate per polymer with > 10 nematodes per experiment, no significant differences in viability were observed (p > 0.05). **C)** Microscope images of nematodes before and after exposure to polymer NPs. Nematode progeny can be seen in control maintenance M9 alone and polymer treated suspensions after 24 h of exposure, indicative of nematode viability.

Table 5
Size, PDI and zeta-potential of Cou6 or MeCou loaded polymer NPs.

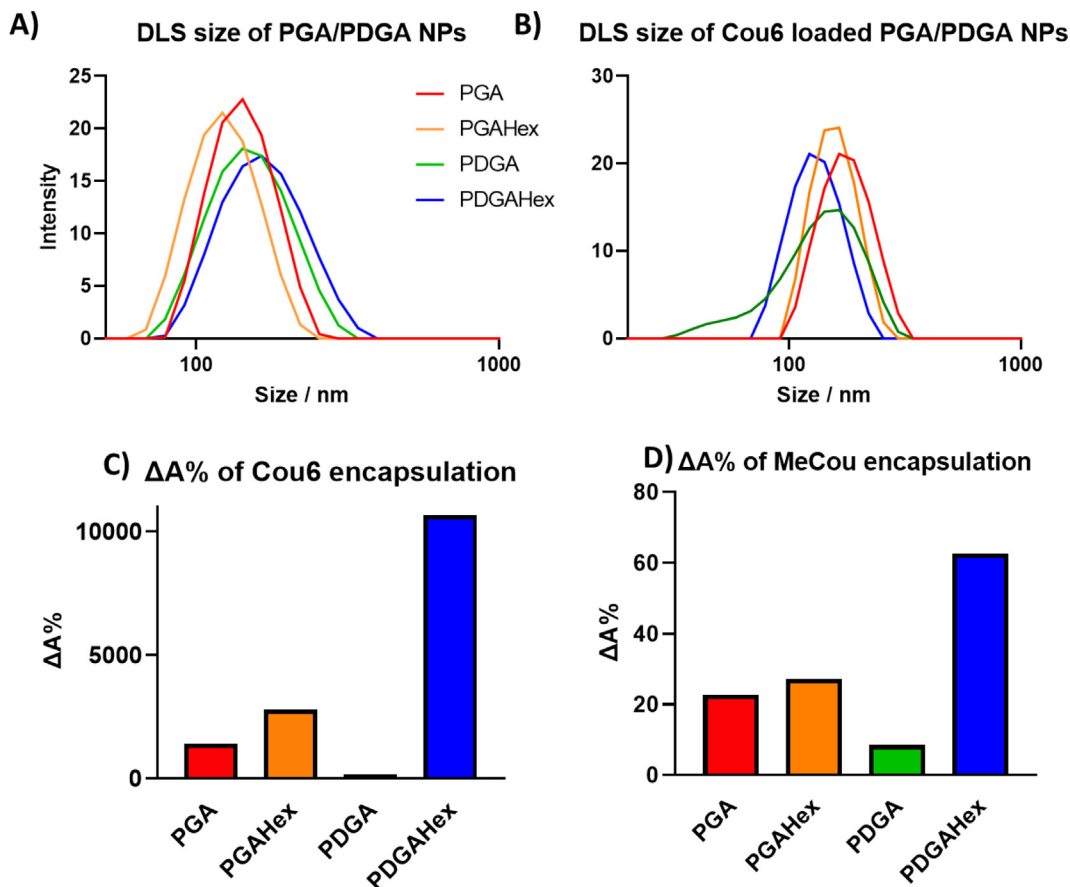| Encapsulated Molecule	Entry	Sample	Average size / nm [a]	PDI [a]	Zeta potential / mV
Cou6	1	PGA	170.2 ± 1.2	0.03 ± 0.01	−24.8 ± 0.8
	2	PDGA	197.7 ± 38.6	0.34 ± 0.10	−18.8 ± 0.1
	3	PGAHex	154.1 ± 1.7	0.04 ± 0.01	−28.4 ± 1.1
	4	PDGAHex	126.6 ± 0.7	0.05 ± 0.02	−26.5 ± 1.6
MeCou	5	PGA	148.0 ± 0.7	0.03 ± 0.02	−22.8 ± 0.2
	6	PDGA	2492.0 ± 0.9	1.00 ± 0.01	−23.2 ± 1.5
	7	PGAHex	133.8 ± 0.5	0.06 ± 0.02	−32.8 ± 0.5
	8	PDGAHex	131.0 ± 0.9	0.05 ± 0.01	−31.3 ± 0.9

[a] Determined by DLS measurements.

Fig. 7. A) Polymer NPs sizes by DLS. **B)** Cou6 loaded NPs sizes by DLS. **C)** ΔA% of Cou6 against PGA, PDGA and modifications. **D)** ΔA% of MeCou against PGA, PDGA and modifications.

the polymer backbone as well as the additional hydroxyl functionalities provided by diglycerol.

The ΔA% values for the MeCou encapsulation were considerably lower that the Cou6 counterparts (22.8, 8.5, 27.2 and 62.6% for PGA, PDGA, PGAHex and PDGAHex respectively (Fig. 7D). This can be explained by the increased solubility of MeCou in water compared to Cou6 initially. Therefore, a lower apparent increase in solubility is observed after encapsulation. In the PGA, PDGA and PGAHex NPs, the average size of the NPs was larger than that of the unloaded NPs, likely a result of the poor interaction between the polymer and the drug. However, PDGAHex NPs showed a contraction in size after the encapsulation of MeCou. This was also observed in the encapsulation of Cou6, and may be attributed to stronger interactions between the polymer chain and the drug molecule. This is in agreement with the measured ΔA% values for the PDGAHex NPs, with this modification giving the highest ΔA%

value for the encapsulation of both Cou6 and MeCou. The measured zeta potential values for the MeCou encapsulated NPS were lower than that of the Cou6 encapsulated NPs. This could be explained by the increased solubility of the drug alone in water which may stabilise the formulation by interacting with both the polymer and the aqueous medium.

3.12. In vivo uptake

Cou6 is a hydrophobic dye with a negligible solubility in aqueous environments, as denoted by its LogP (see Encapsulation study section). Therefore, the polymeric PGAHex and PDGAHex nanoparticles provide a vehicle for Cou6 uptake, by nematode *in vivo* drug delivery model and its transport across biological membranes. The presence of fluorescent signal from the *C. elegans* treated for 24 h with Cou6 encapsulated by PDGAHex and PGAHex NPs suggest
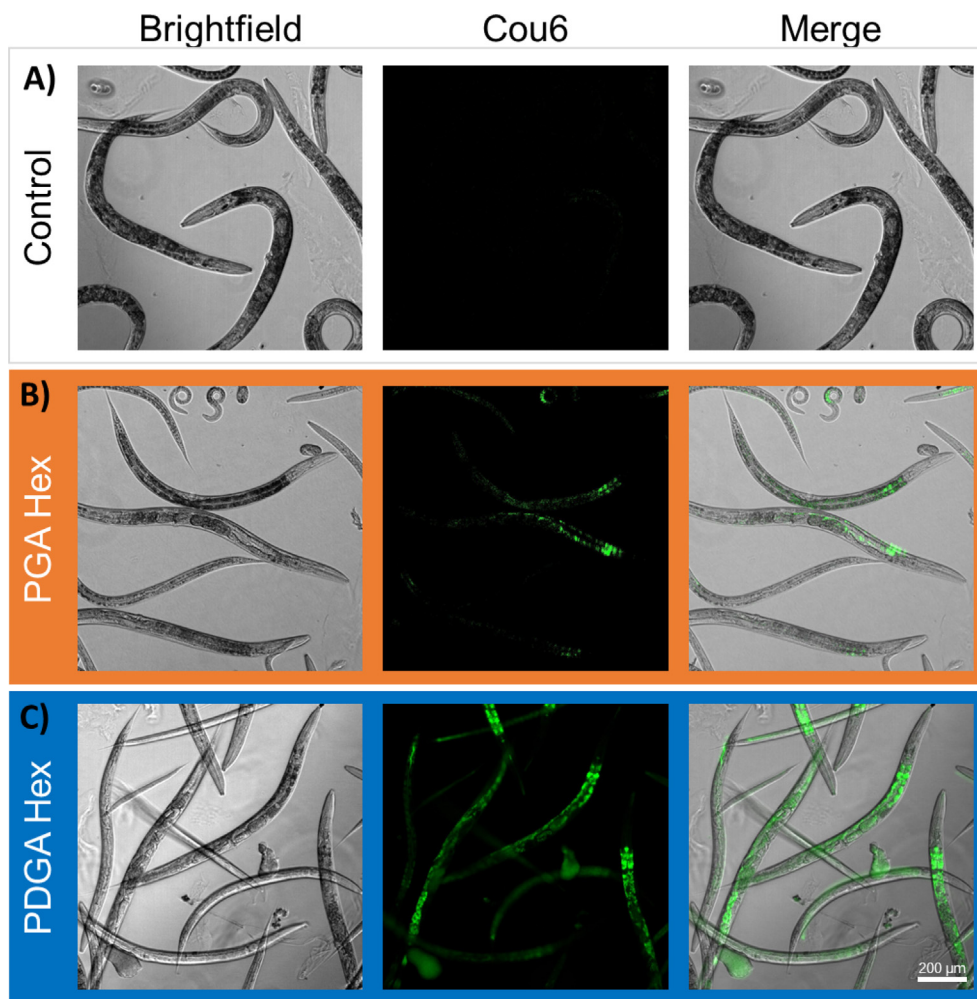
Fig. 8. Fluorescence imaging of *C. elegans* control (M9), PGAHex and PDGAHex treated nematodes (0.5 mg/mL). Baseline fluorescence corrected to 0 green intensity for control. The green intensity dynamic range for PDGAHex images was modified, to be 7 times greater than PGAHex, to overcome pixel saturation. Uptake of Cou6 was observed distributed throughout the nematode anatomy in lipid rich regions. Populations of ~ 200 nematodes were screen for uptake assay. Scale = 200 µm. (For interpretation of the references to colour in this figure legend, the reader is referred to the web version of this article.)

that the NPs were taken up by the nematodes and Cou6 was then delivered across *C. elegans* intestinal membrane (Fig. 8). Specifically, the NPs containing Cou6 distribution in the nematode anatomy appears to localise in lipid droplets adjacent to intestinal track. This observation has been reported with other hydrophobic dye based labelling in nematodes, such as studies with Sudan Black B. [62] The higher propensity of PDGAHex, when compared to PGA-Hex, to encapsulate the hydrophobic Cou6 was also observed in both the encapsulation studies (Fig. 7C) as well as in the uptake studies (Fig. 8B & 8C). To compensate for the enhanced Cou6 uptake with PDGAHex nanoaggregates, with respect to PGAHex data, the green intensity dynamic range of PDGAHex was modified to be 7 times greater, to overcome pixel saturation (Fig. 8B and C **and Experimental Section**). This data indicates polymeric nanoaggregates, specifically PDGAHex, could be used as an effective vehicle to deliver hydrophobic drugs, to simple *in vivo* drug delivery models such as *C. elegans*. They potenially form the basis for the preparation of advanced drug delivery systems to complex biological systems, such as humans.

4. Conclusion

We have demonstrated that through the selection of the starting polyols, both hydrophobic and hydrophilic, the enzymatic syn-

thetic pathway can be exploited as a sustainable, one-pot tool to produce new functional polyesters. An in-depth physico-chemical and biological screening have been adopted to study the behaviours of the polymers (as whole, the water-soluble fraction and final NPs). Among the newly synthesised polymers, the hexanediol modification of poly(diglycerol adipate) has shown superior polymer compared to the well reported PGA. PDGAHex demonstrated greater stability in relevant aqueous environments as well as an increased ability to encapsulate model dyes when compared to the other polymers. This can be rationalised by an improvement in the amphiphilic balance between the hexanediol-adipic hydrophobic portion within the polymer backbone as well as the additional hydroxyl functionalities provided by the diglycerol moiety. The discovered synergistic relationship between the hydrophilic and hydrophobic segments renders this novel material highly suited to pharmaceutical and biomedical applications.

CRediT authorship contribution statement

Philippa L. Jacob: Conceptualization, Methodology, Investigation, Formal analysis, Writing – original draft. **Benedetta Brugnoli:** Methodology, Investigation, Formal analysis. **Alessandra Del Giudice:** Methodology, Investigation, Formal analysis. **Hien Phan:** Methodology, Investigation, Formal analysis. **Veeren M. Chauhan:**

Methodology, Investigation, Formal analysis. **Laura Beckett:** Methodology, Investigation, Formal analysis. **Richard B. Gillis:** Methodology, Investigation, Formal analysis. **Cara Moloney:** Methodology, Investigation, Formal analysis. **Robert J. Cavanagh:** Methodology, Investigation, Formal analysis. **Eduards Krumins:** Methodology, Investigation, Formal analysis. **Morgan Reynolds-Green:** Methodology, Investigation, Formal analysis. **Joachim C. Lentz:** Methodology, Investigation, Formal analysis. **Claudia Conte:** Methodology. **Valentina Cuzzucoli Crucitti:** Methodology, Investigation, Formal analysis. **Benoit Couturaud:** Supervision. **Luciano Galantini:** Supervision. **Iolanda Francolini:** Supervision. **Steven M. Howdle:** Supervision. **Vincenzo Taresco:** Conceptualization, Supervision, Writing – review & editing, Funding acquisition.

Data availability

Data will be made available on request.

Declaration of Competing Interest

The authors declare that they have no known competing financial interests or personal relationships that could have appeared to influence the work reported in this paper.

Acknowledgements

Appendix A. Supplementary data

Supplementary data to this article can be found online at https://doi.org/10.1016/j.jcis.2023.03.124.

References

[1] W. of Science, Results for polymeric nanoparticles drug delivery (All Fields) and 202(Publication Years), https://www.webofscience.com/wos/woscc/analyze-results/7eb186f6-7933-48cb-95ff-88e4539e0a4a-5108a103, (accessed 23 September 2022).

[2] E. Calzoni, A. Cesaretti, A. Polchi, A. Di Michele, B. Tancini, C. Emiliani, J. Funct. Biomater. 10 (2019) 4.

[3] K. E. Washington, R. N. Kularatne, V. Karmegam, M. C. Biewer and M. C. Stefan, *Wiley Interdiscip. Rev. Nanomed. Nanobiotechnol.*, Doi: 10.1002/wnan.1446.

[4] E. Niza, A. Ocaña, J.A. Castro-Osma, I. Bravo, C. Alonso-Moreno, Cancers (Basel) 13 (2021) 3387.

[5] M.J. Mitchell, M.M. Billingsley, R.M. Haley, M.E. Wechsler, N.A. Peppas, R. Langer, Nat. Rev. Drug Discov. 20 (2021) 101–124.

[6] T.T. Hoang Thi, E.H. Pilkington, D.H. Nguyen, J.S. Lee, K.D. Park, N.P. Truong, Polymers 12 (2020) 298.

[7] A. Thomas, S.S. Müller, H. Frey, Biomacromolecules 15 (2014) 1935–1954.

[8] K. Knop, R. Hoogenboom, D. Fischer, U.S. Schubert, Angew. Chem. Int. Ed. 49 (2010) 6288–6308.

[9] Y.K. Sung, S.W. Kim, Biomater. Res. 24 (2020) 12.

[10] R. Langer, Nature 392 (1998) 5–10.

[11] P.K. Samantaray, A. Little, D.M. Haddleton, T. McNally, B. Tan, Z. Sun, W. Huang, Y. Ji, C. Wan, Green Chem. 22 (2020) 4055–4081.

[12] K.J. Jem, B. Tan, Adv. Ind. Eng. Polym. Res. 3 (2020) 60–70.

[13] T. Casalini, F. Rossi, A. Castrovinci, G. Perale, Front. Bioeng. Biotechnol. 7 (2019) 1–16.

[14] B. Tyler, D. Gullotti, A. Mangraviti, T. Utsuki, H. Brem, Adv. Drug Deliv. Rev. 107 (2016) 163–175.

[15] M.S. Singhvi, S.S. Zinjarde, D.V. Gokhale, J. Appl. Microbiol. 127 (2019) 1612–1626.

[16] P.K. Gupta, R. Gahtori, K. Govarthanan, V. Sharma, S. Pappuru, S. Pandit, A.S. Mathuriya, S. Dholpuria, D.K. Bishi, Mater. Sci. Eng. C 127 (2021) 112198.

[17] K.K. Bansal, E. Özliseli, A. Rosling, J.M. Rosenholm, Adv. Funct. Mater. 31 (2021) 2101998.

[18] A.L. Chin, X. Wang, R. Tong, Macromol. Biosci. 21 (2021) 2100087.

[19] C. Dourado Fernandes, B. Francisco Oechsler, C. Sayer, D. de Oliveira, P.H. Hermes de Araújo, Eur. Polym. J. 169 (2022) 111132.

[20] S.M.E. Swainson, I.D. Styliari, V. Taresco, M.C. Garnett, Polymers 11 (2019) 1561.

[21] Á.S. Olalla, V.H. Talavera, D.L. García, E.G. Torres, M.F. García, Eur. Polym. J. 170 (2022) 111173.

[22] S.M.E. Swainson, V. Taresco, A.K. Pearce, L.H. Clapp, B. Ager, M. McAllister, C. Bosquillon, M.C. Garnett, Eur. J. Pharm. Biopharm. 142 (2019) 377–386.

[23] G.M. Lari, G. Pastore, C. Mondelli, J. Pérez-Ramírez, Green Chem. 20 (2018) 148–159.

[24] V. Taresco, R.G. Creasey, J. Kennon, G. Mantovani, C. Alexander, J.C. Burley, M.C. Garnett, Polymer 89 (2016) 41–49.

[25] V.M. Weiss, T. Naolou, G. Hause, J. Kuntsche, J. Kressler, K. Mäder, J. Control. Release 158 (2012) 156–164.

[26] J. Suksiriworapong, V. Taresco, D.P. Ivanov, I.D. Styliari, K. Sakchaisri, V.B. Junyaprasert, M.C. Garnett, Colloids Surfaces B Biointerfaces 167 (2018) 115–125.

[27] P. Kallinteri, S. Higgins, G.A. Hutcheon, C.B. St, Pourçain, M.C. Garnett, Biomacromolecules 6 (2005) 1885–1894.

[28] P.L. Jacob, L.A. Ruiz Cantu, A.K. Pearce, Y. He, J.C. Lentz, J.C. Moore, F. Machado, G. Rivers, E. Apebende, M.R. Fernandez, I. Francolini, R. Wildman, S.M. Howdle, V. Taresco, Polymer 228 (2021) 123912.

[29] S. Puri, P. Kallinteri, S. Higgins, G.A. Hutcheon, M.C. Garnett, J. Control. Release 125 (2008) 59–67.

[30] V. Taresco, J. Suksiriworapong, R. Creasey, J.C. Burley, G. Mantovani, C. Alexander, K. Treacher, J. Booth, M.C. Garnett, J. Polym. Sci. Part A Polym. Chem. 54 (2016) 3267–3278.

[31] V.M. Weiss, T. Naolou, T. Groth, J. Kressler, K. Mäder, J. Appl. Biomater. Funct. Mater. 10 (2012) 163–169.

[32] T. Wersig, R. Krombholz, C. Janich, A. Meister, J. Kressler, K. Mäder, Eur. J. Pharm. Sci. 123 (2018) 350–361.

[33] B. Parshad, R. Kumari, M. Khatri, R. Rajeshwari, Y. Pan, A.K. Sharma, I. Ahmed, Eur. Polym. J. 158 (2021) 110690.

[34] D.M. O'Brien, R.L. Atkinson, R. Cavanagh, A.A.C. Pacheco, R. Larder, K. Kortsen, E. Krumins, A.J. Haddleton, C. Alexander, R.A. Stockman, S.M. Howdle, V. Taresco, Eur. Polym. J. 125 (2020) 109516.

[35] V. Cuzzucoli Crucitti, L. Contreas, V. Taresco, S.C. Howard, A.A. Dundas, M.J. Limo, T. Nisisako, P.M. Williams, P. Williams, M.R. Alexander, R.D. Wildman, B.W. Muir, D.J. Irvine, ACS Appl. Mater. Interfaces 13 (2021) 43290–43300.

[36] P. Schuck, R.B. Gillis, T.M.D. Besong, F. Almutairi, G.G. Adams, A.J. Rowe, S.E. Harding, Analyst 139 (2014) 79–92.

[37] R.D.C. Cruz, R.J. Martins, M.J.E. de, M. Cardoso, O.E. Barcia, J. Solution Chem. 38 (2009) 957–981.

[38] I. Breßler, J. Kohlbrecher, A.F. Thünemann, J. Appl. Crystallogr. 48 (2015) 1587–1598.

[39] K. Manalastas-Cantos, P.V. Konarev, N.R. Hajizadeh, A.G. Kikhney, M.V. Petoukhov, D.S. Molodenskiy, A. Panjkovich, H.D.T. Mertens, A. Gruzinov, C. Borges, C.M. Jeffries, D.I. Svergun, D. Franke, J. Appl. Crystallogr. 54 (2021) 343–355.

[40] M. Sanna, G. Sicilia, A. Alazzo, N. Singh, F. Musumeci, S. Schenone, K.A. Spriggs, J.C. Burley, M.C. Garnett, V. Taresco, C. Alexander, A.C.S. Med, Chem. Lett. 9 (2018) 193–197.

[41] T. Stiernagle, in *WormBook*, ed. T. C. elegans R. Community, 2006, pp. 1–11.

[42] V.M. Chauhan, G. Orsi, A. Brown, D.I. Pritchard, J.W. Aylott, ACS Nano 7 (2013) 5577–5587.

[43] H. Uyama, K. Inada, S. Kobayashi, Macromol. Biosci. 1 (2001) 40–44.

[44] A. Thiesen, C. Johann, M.P. Deacon, S.E. Harding, Refractive Increment Data-Book, Nottingham University Press, Nottingham, 2000.

[45] R.G.M. van der Sman, J. Phys. Chem. B 117 (2013) 16303–16313.

[46] A. Khalyavina, L. Häußler, A. Lederer, Polymer 53 (2012) 1049–1053.

[47] E. Álvarez-Castillo, S. Oliveira, C. Bengoechea, I. Sousa, A. Raymundo, A. Guerrero, J. Food Eng. 288 (2021) 110255.

[48] P. Eaton, P. Quaresma, C. Soares, C. Neves, M.P. de Almeida, E. Pereira, P. West, Ultramicroscopy 182 (2017) 179–190.

[49] C.I.C. Crucho, M.T. Barros, Mater. Sci. Eng. C 80 (2017) 771–784.

[50] C.E. Vasey, A.K. Pearce, F. Sodano, R. Cavanagh, T. Abelha, V. Cuzzucoli Crucitti, A.B. Anane-Adjei, M. Ashford, P. Gellert, V. Taresco, C. Alexander, V.C. Crucitti, A.B. Anane-Adjei, M. Ashford, P. Gellert, V. Taresco, C. Alexander, Biomater. Sci. 7 (2019) 3832–3845.

[51] B.J. Kline, E.J. Beckman, A.J. Russell, J. Am. Chem. Soc. 120 (1998) 9475–9480.

[52] C. Graf, Q. Gao, I. Schütz, C.N. Noufele, W. Ruan, U. Posselt, E. Korotianskiy, D. Nordmeyer, F. Rancan, S. Hadam, A. Vogt, J. Lademann, V. Haucke, E. Rühl, Langmuir 28 (2012) 7598–7613.

[53] H. Phan, R.I. Minut, P. McCrorie, C. Vasey, R.R. Larder, E. Krumins, M. Marlow, R. Rahman, C. Alexander, V. Taresco, A.K. Pearce, J. Polym. Sci. Part A Polym. Chem. 57 (2019) 1801–1810.

[54] H.T.M. Phan, S. Bartelt-Hunt, K.B. Rodenhausen, M. Schubert, J.C. Bartz, PLoS One 10 (2015) e0141282.

[55] G.S. Greschner, Die Makromol. Chemie 170 (1973) 203–229.

[56] P. Lindner, T. Zemb, eds., Neutron, X-rays and Light. Scattering Methods Applied to Soft Condensed Matter, 1st ed., North Holland, Amsterdam, 2002. https://doi.org/10.1016/s1369-7021(02)01143-4.

[57] M.A. Al-Natour, M.D. Yousif, R. Cavanagh, A. Abouselo, E.A. Apebende, A. Ghaemmaghami, D.-H. Kim, J.W. Aylott, V. Taresco, V.M. Chauhan, C. Alexander, ACS Macro Lett. 9 (2020) 431–437.

[58] Coumarin 6 | C20H18N2O2S - PubChem, https://pubchem.ncbi.nlm.nih.gov/compound/Coumarin-6#section=Computed-Properties, (accessed 21 November 2022).

[59] 4-Methylesculetin | C10H8O4 - PubChem, https://pubchem.ncbi.nlm.nih.gov/compound/5319502#section=Computed-Properties, (accessed 21 November 2022).

[60] I. Rivolta, A. Panariti, B. Lettiero, S. Sesana, P. Gasco, M.R. Gasco, M. Masserini, G. Miserocchi, J. Physiol. Pharmacol. 62 (2011) 45–53.

[61] A. Trapani, J. Sitterberg, U. Bakowsky, T. Kissel, Int. J. Pharm. 375 (2009) 97–106.

[62] K.D. Kimura, H.A. Tissenbaum, Y. Liu, G. Ruvkun, Science (80-.) 277 (1997) 942–946.